Supporting Information for:

Oligomer formation from the gas-phase reactions of Criegee intermediates with hydroperoxide esters: mechanism and kinetics

Long Chen,[1,2] Yu Huang,*[,1,2] Yonggang Xue,[1,2] Zhihui Jia,[3] Wenliang Wang[4]

[1] *State Key Lab of Loess and Quaternary Geology (SKLLQG), Institute of Earth Environment, Chinese Academy of Sciences (CAS), Xi'an, 710061, China*

[2] *CAS Center for Excellence in Quaternary Science and Global Change, Xi'an, 710061, China*

[3] *School of Materials Science and Engineering, Shaanxi Normal University, Xi'an, Shaanxi, 710119, China*

[4] *School of Chemistry and Chemical Engineering, Key Laboratory for Macromolecular Science of Shaanxi Province, Shaanxi Normal University, Xi'an, Shaanxi, 710119, China*

Submitted to *Atmospheric Chemistry & Physics*

*Corresponding author:

Prof. Yu Huang, E-mail address: huangyu@ieecas.cn

Contents:

Table S1 The electronic energy ($\Delta E^{\neq}$) and Gibbs free energy ($\Delta G^{\neq}$) barriers for the initial reactions of distinct SCIs with HCOOH predicted at the Y/X (Y = M06-2X, CCSD(T) and QCISD(T), X = ma-TZVP, 6-311+G(2df,2p) level based on the M06-2X/6-311+G(2df,2p) optimized geometries (kcal mol^{-1})

	M06-2X/ ma-TZVP		CCSD(T)/ 6-311+G(2df,2p)		QCISD(T)/ 6-311+G(2df,2p)	
	$\Delta E^{\neq}$	$\Delta G^{\neq}$	$\Delta E^{\neq}$	$\Delta G^{\neq}$	$\Delta E^{\neq}$	$\Delta G^{\neq}$
Entry 2						
CH_2OO	8.0	10.0	8.6	10.5	8.7	10.7
anti-CH_3CHOO	12.0	13.0	11.0	11.9	10.9	12.0
syn-CH_3CHOO	13.1	14.6	13.3	14.9	13.2	14.8
Entry 3						
CH_2OO	20.6	21.8	20.4	21.6	20.6	21.8
anti-CH_3CHOO	20.6	22.2	20.2	21.8	20.2	21.8
syn-CH_3CHOO	25.7	27.6	25.6	27.7	25.8	27.7
Entry 4						
CH_2OO	4.4	5.8	4.2	5.6	4.3	5.7
anti-CH_3CHOO	4.1	5.6	3.3	4.9	3.4	4.9
syn-CH_3CHOO	8.9	11.1	8.5	10.9	8.6	10.8

Table S2 Rate coefficients (cm^3 $molecule^{-1}$ s^{-1}) of each elementary pathway involved in the initiation reaction of CH_2OO with HCOOH computed at different temperatures

T/K	*k* (TSent1)	*k* (TSent2)	*k* (TSent3)	*k* (TSent4)	k_{tot}
273	4.3×10^{-10}	3.6×10^{-12}	1.0×10^{-22}	3.6×10^{-12}	4.3×10^{-10}
280	3.8×10^{-10}	2.9×10^{-12}	1.2×10^{-22}	3.1×10^{-12}	3.9×10^{-10}
298	3.6×10^{-10}	1.9×10^{-12}	2.2×10^{-22}	2.3×10^{-12}	3.6×10^{-10}
300	3.5×10^{-10}	1.8×10^{-12}	2.4×10^{-22}	2.2×10^{-12}	3.5×10^{-10}
320	2.9×10^{-10}	1.2×10^{-12}	4.9×10^{-22}	1.6×10^{-12}	2.9×10^{-10}
340	2.8×10^{-10}	8.2×10^{-13}	1.0×10^{-21}	1.3×10^{-12}	2.8×10^{-10}
360	2.6×10^{-10}	5.9×10^{-13}	2.2×10^{-21}	1.0×10^{-12}	2.6×10^{-10}
380	2.4×10^{-10}	4.5×10^{-13}	4.5×10^{-21}	8.2×10^{-13}	2.4×10^{-10}
400	2.1×10^{-10}	3.5×10^{-13}	9.0×10^{-21}	6.9×10^{-13}	2.1×10^{-10}

Table S3 Rate coefficients (cm^3 $molecule^{-1}$ s^{-1}) of each elementary pathway involved in the initiation reaction of *anti*-CH_3CHOO with HCOOH computed at different temperatures

T/K	k (TS_{ent1}-*anti*)	k (TS_{ent2}-*anti*)	k (TS_{ent3}-*anti*)	k (TS_{ent4}-*anti*)	k (tot-*anti*)
273	9.7×10^{-10}	4.2×10^{-11}	5.5×10^{-22}	6.1×10^{-11}	1.1×10^{-9}
280	9.5×10^{-10}	3.8×10^{-11}	6.7×10^{-22}	4.9×10^{-11}	1.0×10^{-9}
298	9.3×10^{-10}	2.3×10^{-11}	1.2×10^{-21}	3.0×10^{-11}	9.8×10^{-10}
300	9.2×10^{-10}	2.0×10^{-11}	1.3×10^{-21}	2.8×10^{-11}	9.7×10^{-10}
320	8.6×10^{-10}	1.5×10^{-11}	2.6×10^{-21}	1.7×10^{-11}	8.9×10^{-10}
340	8.3×10^{-10}	9.4×10^{-12}	5.4×10^{-21}	1.1×10^{-11}	8.5×10^{-10}
360	8.2×10^{-10}	7.0×10^{-12}	1.1×10^{-20}	7.8×10^{-12}	8.3×10^{-10}
380	8.1×10^{-10}	3.6×10^{-12}	2.1×10^{-20}	5.6×10^{-12}	8.2×10^{-10}
400	8.1×10^{-10}	2.0×10^{-12}	4.0×10^{-20}	4.2×10^{-12}	8.2×10^{-10}

Table S4 Rate coefficients (cm^3 $molecule^{-1}$ s^{-1}) of each elementary pathway involved in the initiation reaction of *syn*-CH_3CHOO with HCOOH computed at different temperatures

T/K	k (TS_{ent1}-*syn*)	k (TS_{ent2}-*syn*)	k (TS_{ent3}-*syn*)	k (TS_{ent4}-*syn*)	k (tot-*syn*)
273	7.7×10^{-10}	9.5×10^{-13}	4.6×10^{-27}	7.5×10^{-16}	7.7×10^{-10}
280	7.4×10^{-10}	8.0×10^{-13}	7.1×10^{-27}	6.4×10^{-16}	7.4×10^{-10}
298	7.2×10^{-10}	5.4×10^{-13}	8.9×10^{-26}	5.5×10^{-16}	7.2×10^{-10}
300	7.1×10^{-10}	5.2×10^{-13}	9.9×10^{-26}	4.6×10^{-16}	7.1×10^{-10}
320	6.8×10^{-10}	3.6×10^{-13}	3.0×10^{-25}	3.8×10^{-16}	6.8×10^{-10}
340	6.5×10^{-10}	2.6×10^{-13}	9.1×10^{-25}	3.1×10^{-16}	6.5×10^{-10}
360	6.3×10^{-10}	2.0×10^{-13}	2.6×10^{-24}	3.0×10^{-16}	6.3×10^{-10}
380	6.2×10^{-10}	1.5×10^{-13}	7.2×10^{-24}	2.4×10^{-16}	6.2×10^{-10}
400	6.1×10^{-10}	1.2×10^{-13}	1.8×10^{-23}	2.2×10^{-16}	6.1×10^{-10}

Table S5 Rate coefficients (cm^3 $molecule^{-1}$ s^{-1}) of each elementary pathway involved in the initiation reaction of $(CH_3)_2OO$ with HCOOH computed at different temperatures

T/K	k (TS_{ent1}-*dim*)	k (TS_{ent2}-*dim*)	k (TS_{ent3}-*dim*)	k (TS_{ent4}-*dim*)	k (tot-*dim*)
273	5.6×10^{-10}	6.8×10^{-12}	1.4×10^{-26}	4.4×10^{-15}	5.7×10^{-10}
280	5.3×10^{-10}	5.2×10^{-12}	2.2×10^{-26}	4.2×10^{-15}	5.4×10^{-10}
298	5.1×10^{-10}	2.8×10^{-12}	7.9×10^{-26}	4.0×10^{-15}	5.1×10^{-10}
300	5.1×10^{-10}	2.6×10^{-12}	9.2×10^{-26}	3.9×10^{-15}	5.1×10^{-10}
320	4.9×10^{-10}	1.4×10^{-12}	3.6×10^{-25}	3.7×10^{-15}	4.9×10^{-10}
340	4.8×10^{-10}	8.6×10^{-13}	1.3×10^{-24}	3.6×10^{-15}	4.8×10^{-10}
360	4.7×10^{-10}	5.5×10^{-13}	4.5×10^{-24}	3.5×10^{-15}	4.7×10^{-10}
380	4.5×10^{-10}	3.7×10^{-13}	1.4×10^{-23}	3.4×10^{-15}	4.5×10^{-10}
400	4.4×10^{-10}	2.6×10^{-13}	3.9×10^{-23}	3.4×10^{-15}	4.4×10^{-10}

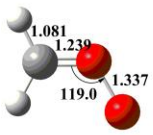

CH_2OO

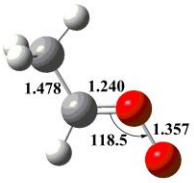

anti-CH_3CHOO

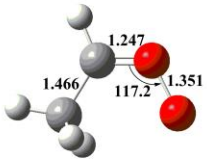

syn-CH_3CHOO

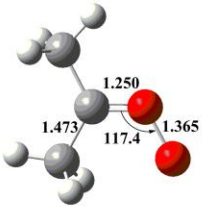

$(CH_3)_2CHOO$

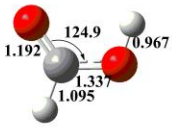

HCOOH

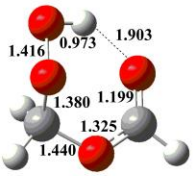

Pent1a

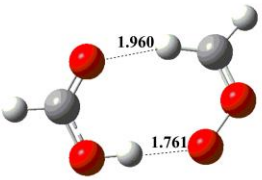

IMent2a

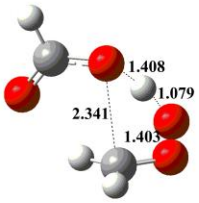

TSent2a

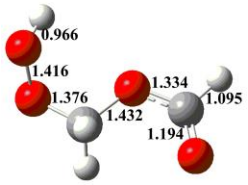

Pent2a

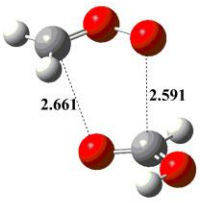

IMent3a

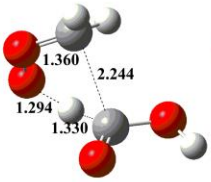

TSent3a

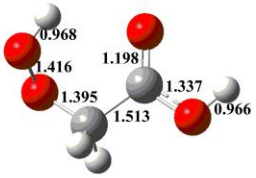

Pent3a

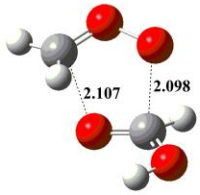

TSent4a

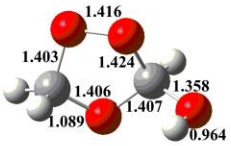

Pent4a

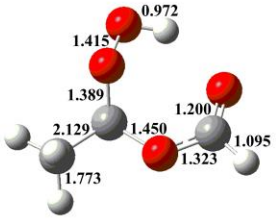

Pent1b

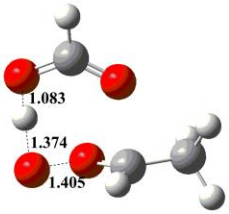

IMent2b

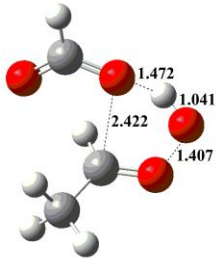

TSent2b

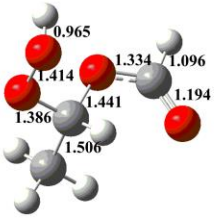

Pent2b

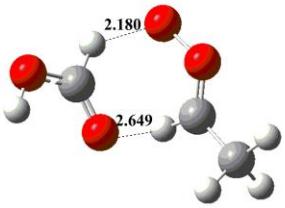

IMent3b

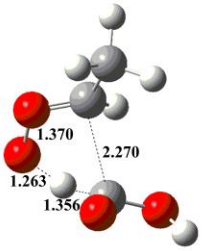

TSent3b

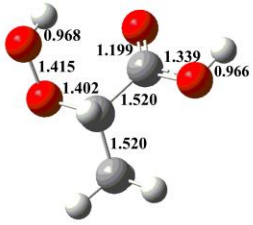

Pent3b

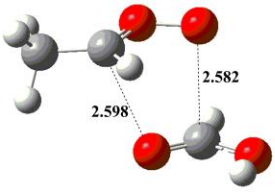

IMent4b

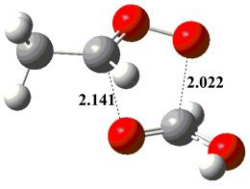

TSent4b

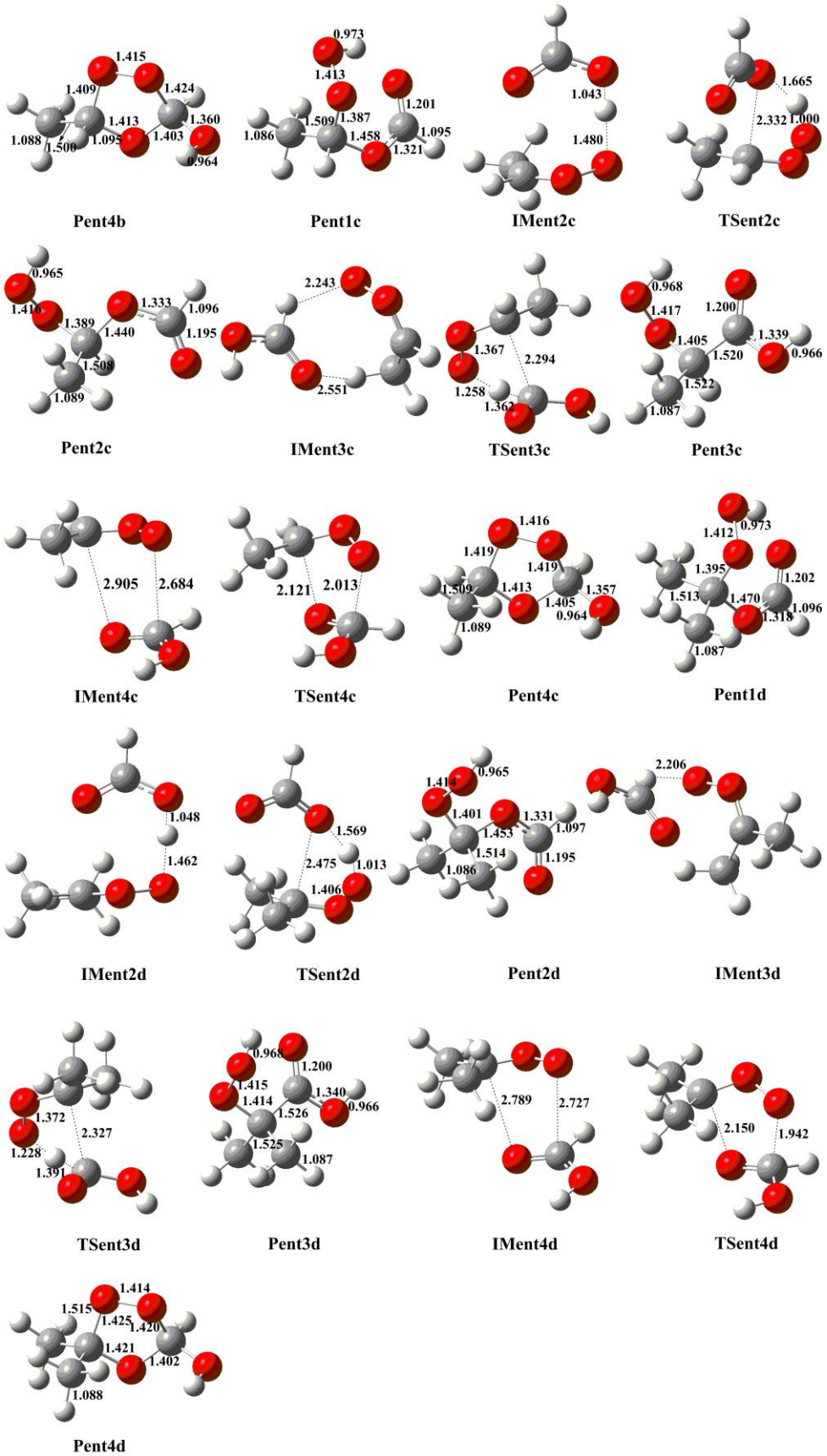

Figure S1. The geometries of all the stationary points for distinct SCIs reactions with formic acid optimized at the M06-2X/6-311+G(2df,2p) level of theory

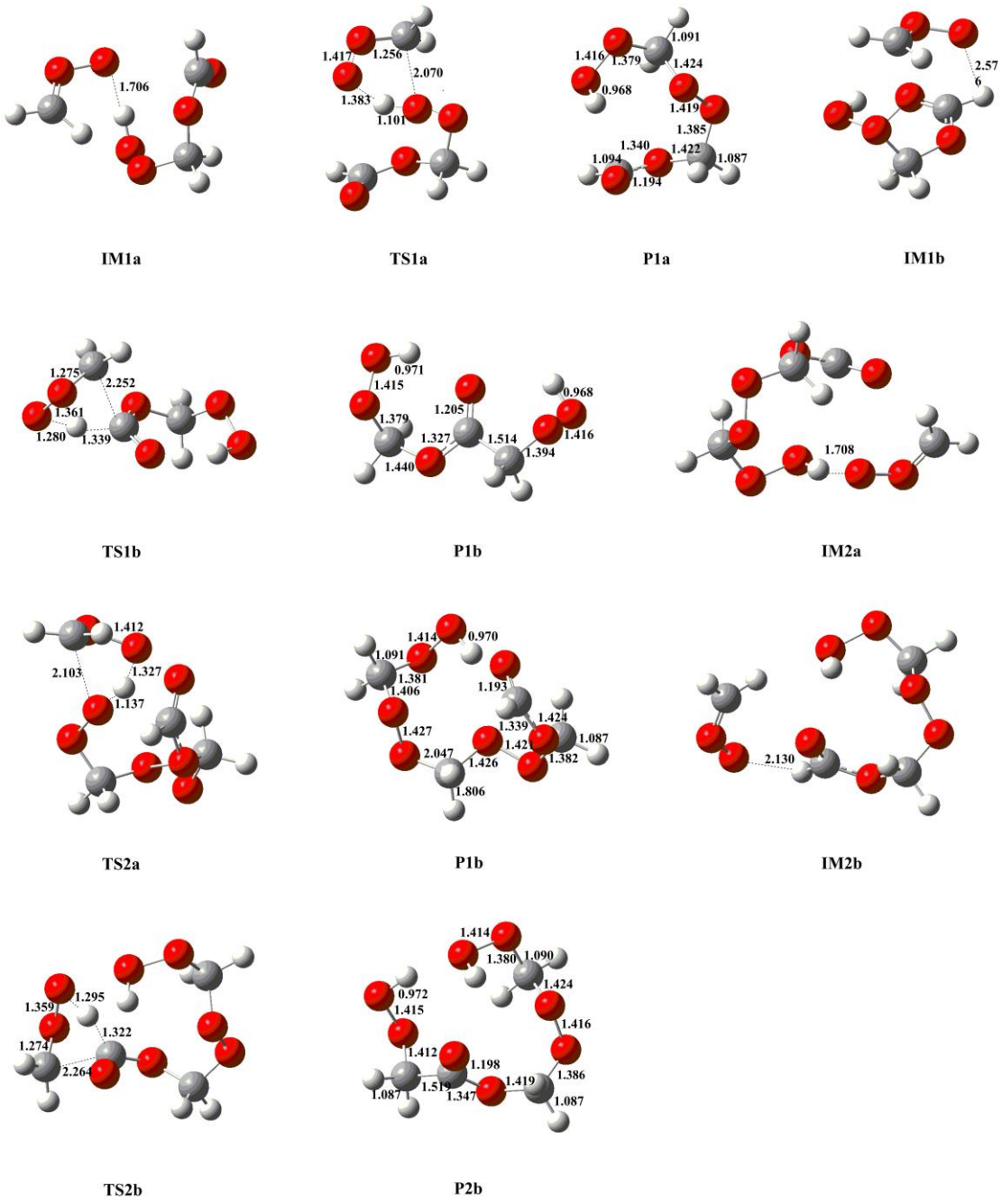

Figure S2. The geometries of all the stationary points for $2CH_2OO$ + Pent1a reaction optimized at the M06-2X/6-311+G(2df,2p) level of theory

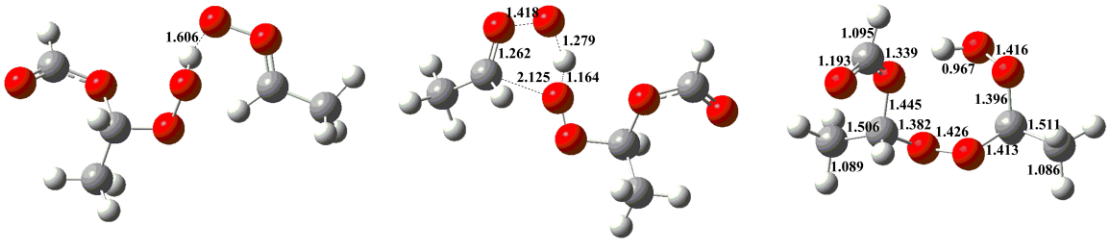

IM3a

TS3a

P3a

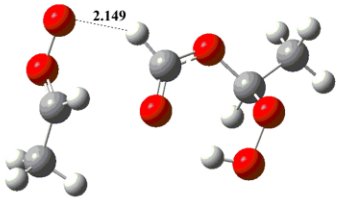

IM3b

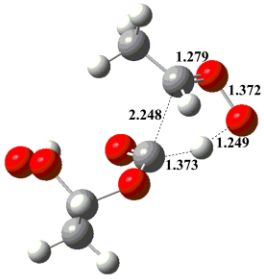

TS3b

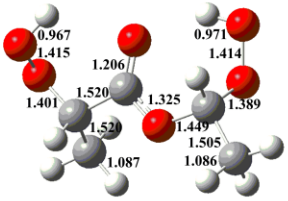

P3b

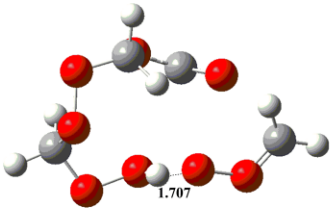

IM4a

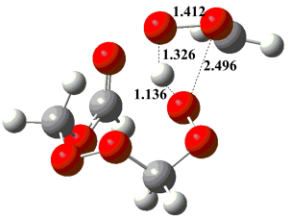

TS4a

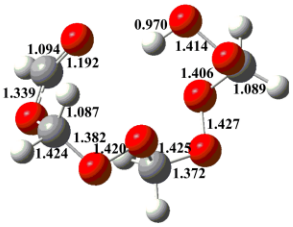

P4a

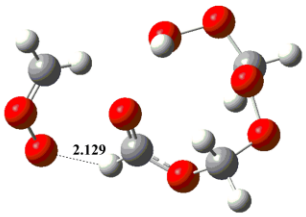

IM4b

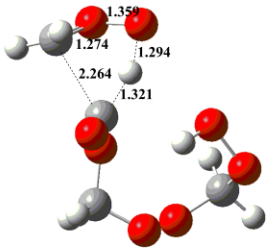

TS4b

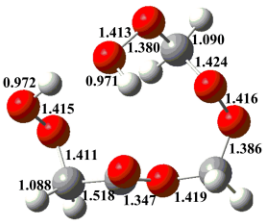

P4b

Figure S3. The geometries of all the stationary points for 2*anti*-CH_3CHOO + Pent1b reaction optimized at the M06-2X/6-311+G(2df,2p) level of theory

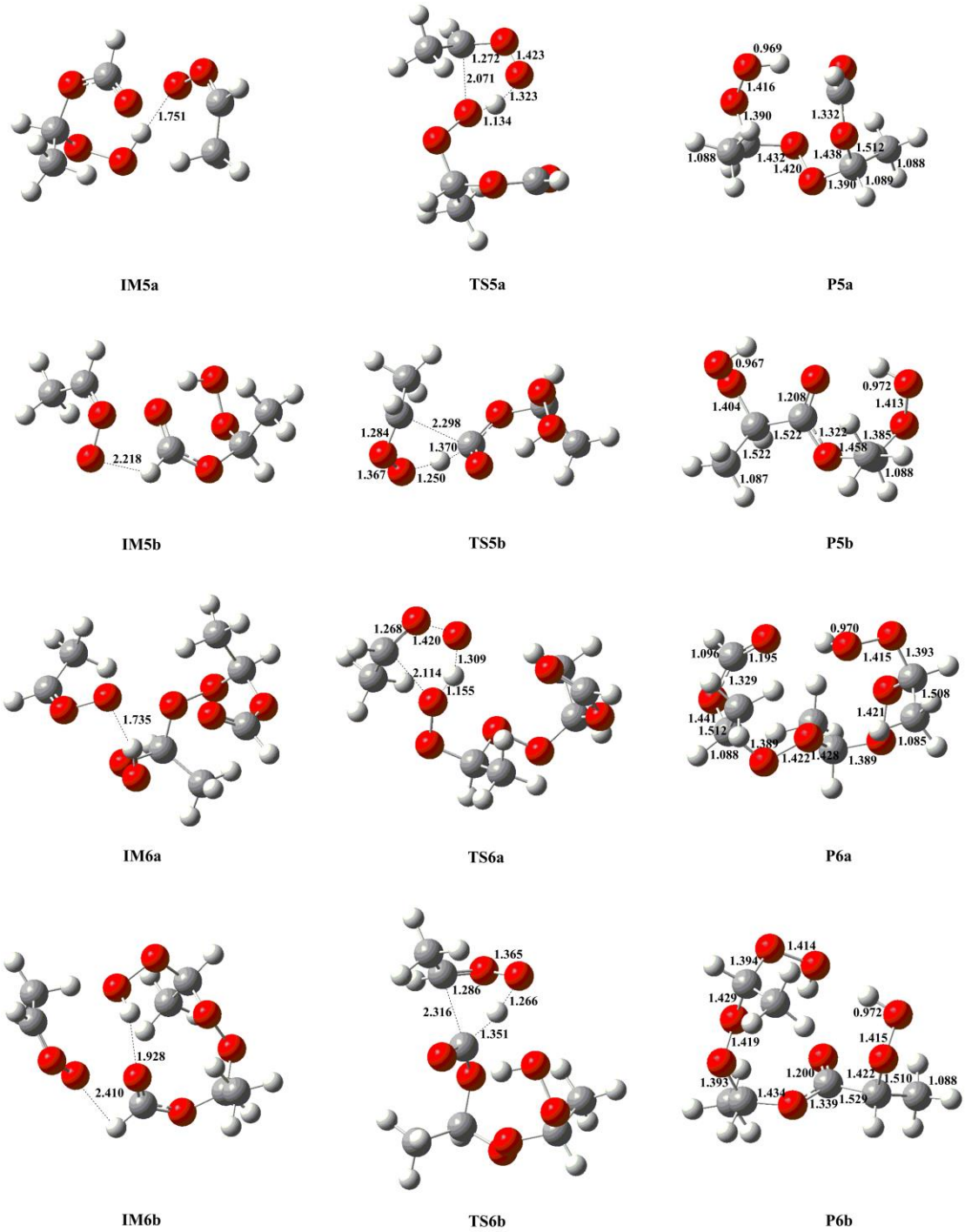

Figure S4. The geometries of all the stationary points for 2*syn*-CH_3CHOO + Pent1c reaction optimized at the M06-2X/6-311+G(2df,2p) level of theory

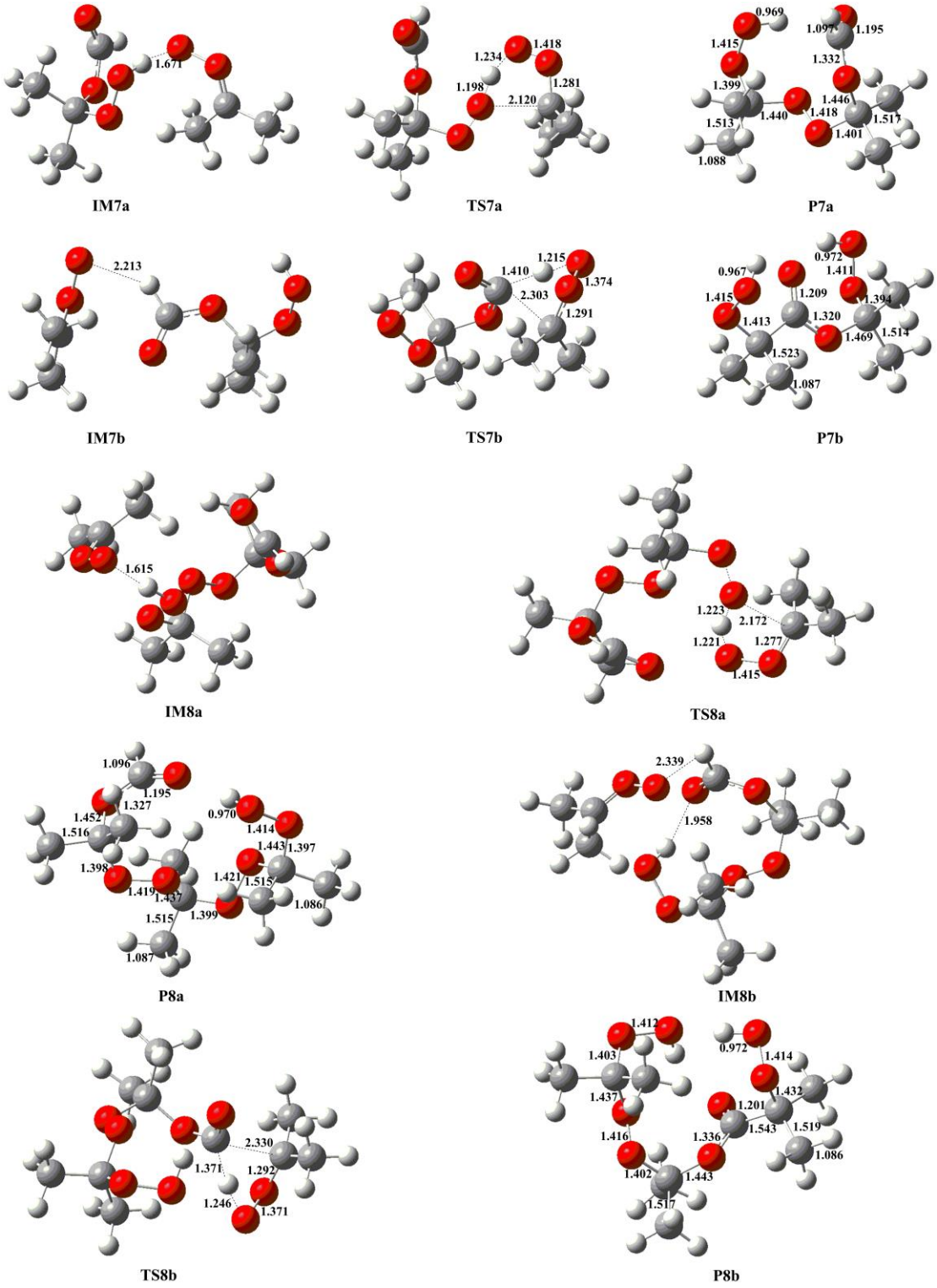

Figure S5. The geometries of all the stationary points for $2(CH_3)_2COO$ + Pent1d reaction optimized at the M06-2X/6-311+G(2df,2p) level of theory

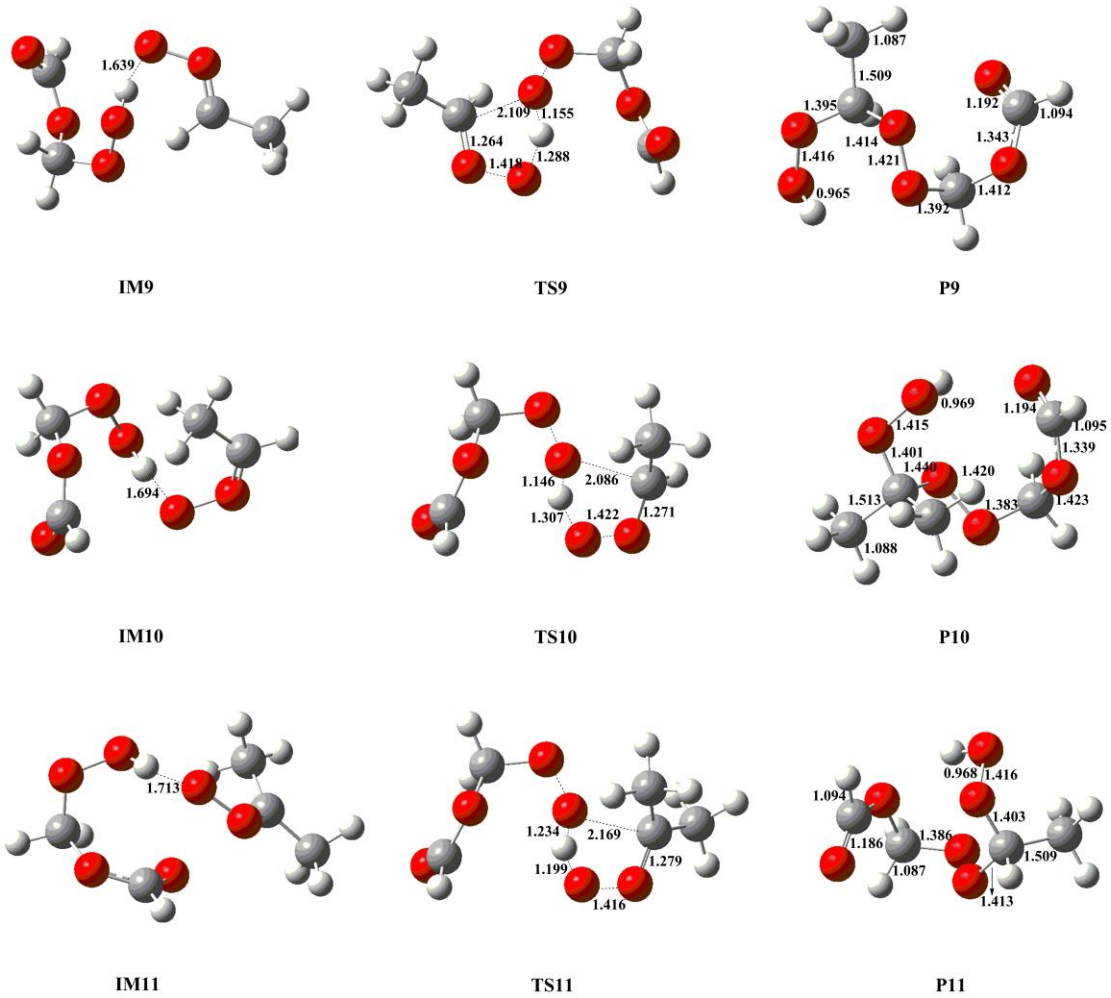

Figure S6. The geometries of all the stationary points for distinct SCIs reactions with Pent1a optimized at the M06-2X/6-311+G(2df,2p) level of theory